

Two-dimensional metallic (Tl, Au)/Si(100)c(2 × 2): A Rashba-type system with C_{2v} symmetryD. V. Gruznev,¹ L. V. Bondarenko,¹ A. Y. Tupchaya,¹ V. G. Kotlyar,¹ O. A. Utas,¹ A. N. Mihalyuk,^{1,2}
S. V. Eremeev,^{3,4} A. V. Zotov,^{1,2} and A. A. Saranin^{1,2}¹*Institute of Automation and Control Processes FEB RAS, 690041 Vladivostok, Russia*²*School of Natural Sciences, Far Eastern Federal University, 690091 Vladivostok, Russia*³*Institute of Strength Physics and Materials Science SB RAS, 634055 Tomsk, Russia*⁴*Tomsk State University, 634050 Tomsk, Russia*

(Received 10 July 2018; published 28 September 2018)

A highly ordered (Tl, Au)/Si(100)c(2 × 2) two-dimensional compound was found to form upon room-temperature adsorption of 1.0 monolayer (ML) of Au onto a Tl/Si(100)2 × 1 surface with 1.0 ML of Tl. The compound was determined to have a double-atomic-layer structure where Au and Tl atoms constitute the bottom and top layers, respectively. The compound is metallic due to the presence of the two dispersive surface-state bands crossing the Fermi level. The bands are spin split, and the peculiar feature of their spin texture is the occurrence of exclusively in-plane spin components that is originated from the C_{2v} symmetry of the system. One of the bands has a typical vortical spin texture, whereas the other exhibits an unusual nonvortical spin texture.

DOI: [10.1103/PhysRevB.98.125428](https://doi.org/10.1103/PhysRevB.98.125428)**I. INTRODUCTION**

Metal-induced surface reconstructions on silicon (i.e., silicon substrates covered with ordered metal films of a monolayer or submonolayer thickness) have attracted considerable attention due to a variety of structural and electronic properties. Because of the current demand for searching advanced materials for prospective spintronics, the very recent interest has been focused on the reconstructions induced by heavy metals (e.g., Tl, Bi, Pt, Au, etc.) where noticeable spin polarization of the electron surface-state bands becomes possible due to the spin-orbit coupling (SOC) concomitant with the breaking of space inversion symmetry along the surface normal. For the ideal two-dimensional (2D) nearly free-electron gas systems, the spins of the split bands are locked in plane and oriented perpendicular to the electron momentum parallel to the surface as described by the simple Rashba [1] and Bychkov-Rashba [2] models. However, the situation is different in real systems where spins might change their direction to out of plane due to the presence of in-plane potential gradients. The spin texture of the split bands is dictated by the atomic structure and lattice symmetry of the given system. Therefore, studies on surfaces with various symmetries are indispensable for the proper understanding of the Rashba effect.

Almost all recent studies of the Rashba effect have been conducted on the Si(111) surface having C_{3v} symmetry where the spin textures of the adsorbed monolayers of Tl [3–12] and Bi [9,13–16] have been explored in great detail. To our knowledge, the studies on the other surfaces are limited by the two researches conducted on the Si(110) surface that have C_{1h} symmetry. These works were devoted to the layers of Pt [17] and Tl [18]. In particular, it has been found that in the Tl/Si(110) system the nonvortical spin structure is realized as a result of the C_{1h} symmetry and such a spin structure is proclaimed to be insensitive to backscattering and therefore to

ensure long coherence [18]. The occurrence of the nonvortical spin texture has been also predicted theoretically for the 2D states belonging to the C_{2v} symmetry [19].

It is worth noting that, when speaking about prospective spintronic applications based on the Rashba effect, one has to bear in mind that the spin-split bands should be metallic, that would allow significant spin transport [20]. Meanwhile, the single-adsorbate reconstructions on silicon almost exclusively possess spin-split insulating bands. Fortunately, the method to create spin-split metallic bands on silicon has been elaborated which resides in growing a dense 2D compound layer containing a metal with strong atomic SOC and another metal to modify the surface reconstruction [21]. The efficiency of the method has been proved by the creation of a set of various 2D compounds with spin-split metallic surface-state bands having various spin textures [22].

In the present paper, this method has been applied to synthesize the Tl-Au 2D compound on the Si(100) surface that has C_{2v} symmetry. The compound has been found to have c(2 × 2) periodicity and a relatively simple double-atomic-layer structure where Au and Tl atoms constitute the bottom and top layers, respectively. It is metallic due to the presence of the two dispersive surface-state bands crossing the Fermi level. Both bands are spin split, and the characteristic feature of their spin textures is the absence of the out-of-plane spin component that stems from the C_{2v} symmetry of the system. The difference between the two bands is that one band has a vortical spin structure, whereas the spin texture of the other is nonvortical.

II. EXPERIMENTAL AND CALCULATION DETAILS

The experiments were conducted in the UHV Omicron MULTIPROBE system equipped with low-energy electron diffraction (LEED), scanning tunnel microscope (STM), and angle-resolved photoemission spectroscopy (ARPES)

facilities. Atomically clean Si(100) 2×1 surfaces were prepared *in situ* by flashing to 1250 °C for 25 s after the samples were first annealed at 830 °C for 1 h. Thallium and gold were deposited from a Ta tube and from a W filament, respectively. STM images were acquired in a constant-current mode with a mechanically cut PtIr tip after annealing in vacuum. ARPES measurements were conducted using a VG Scienta R3000 electron analyzer and a high-flux He discharge lamp with a toroidal-grating monochromator as a light source.

Our calculations were based on density functional theory (DFT) as implemented in the Vienna *ab initio* simulation package [23,24] using a plane-wave basis set. The projector-augmented-wave approach [25] was used to describe the electron-ion interaction. The local density approximation (LDA) [26] for an exchange-correlation functional was employed for structure optimization and the establishment of the surface reconstruction with using the *ab initio* random structure searching (AIRSS) approach [27]. To simulate the Tl-Au reconstructions on Si(100), we used a slab consisting of 60 single layers (SLs) of silicon for the LDA-optimized bulk Si lattice constant. Hydrogen atoms were used to passivate the Si dangling bonds at the bottom of the slab. The atomic positions of adsorbed atoms and atoms of Si layers within the six SLs of the slab were optimized. Silicon atoms of the deeper layers were kept fixed at the bulk crystalline positions. The geometry optimization was performed until the residual force on the atoms was smaller than 10 meV/Å. For band-structure calculations we used both the LDA and the hybrid functional approach of Heyd, Scuseria, and Ernzerhof (HSE06) [28]. Within the LDA, we applied an approximate quasiparticle approach LDA-1/2 [29,30] to improve the Si band gap. In the HSE06 calculation a slab of reduced thickness, consisting of 20 Si SLs, was used. The kinetic cutoff energy was 250 eV, and a $12 \times 12 \times 1$ k -point mesh was used to sample the surface Brillouin zone (SBZ).

III. RESULTS AND DISCUSSION

The formation of the highly ordered (Tl, Au)/Si(100) $c(2 \times 2)$ compound was started with the preparation of the atomically clean two-domain Si(100) 2×1 surface with the minimal density of surface defects, missing dimers, and C defects [Figs. 1(a) and 1(b)]. Thallium adsorption onto this surface held at room-temperature (RT) results in the formation of the Tl/Si(100) 2×1 phase [Figs. 1(c) and 1(d)] which incorporates 1.0 monolayer (ML, $6.8 \times 10^{14} \text{ cm}^{-2}$) of Tl atoms arranged in the structure described by the pedestal + valley-bridge model [31,32]. The subsequent RT deposition of 1.0 ML of Au leads to the developing (Tl, Au)/Si(100) $c(2 \times 2)$ compound [Figs. 1(e) and 1(f)]. The formed (Tl, Au)/Si(100) $c(2 \times 2)$ compound was found to be thermally stable up to ~ 350 °C.

In order to establish a structural model of the (Tl, Au)/Si(100) $c(2 \times 2)$ compound, we performed DFT calculations in the framework of the *ab initio* random structure searching (AIRSS) technique [27]. The calculations revealed that the lowest-energy (Tl, Au)/Si(100) system incorporates 1.0 ML of Tl and 1.0 ML of Au with Au atoms preferring to make direct bonding with Si atoms.

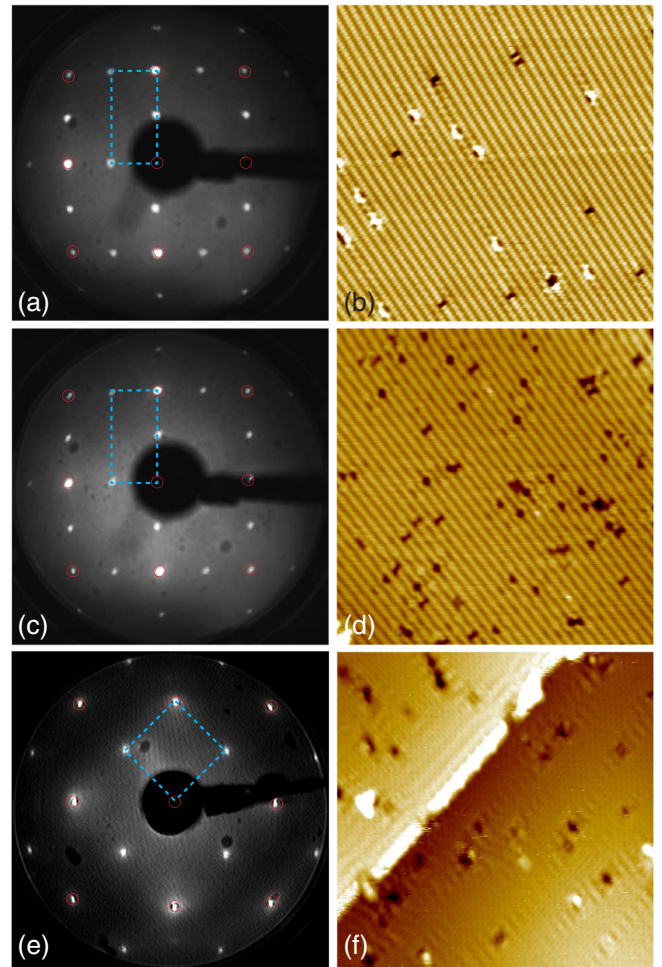


FIG. 1. LEED patterns and 350×350 -Å² filled-state STM images of the (a) and (b) pristine Si(100) 2×1 surface, the (c) and (d) Tl/Si(100) 2×1 phase, and the (e) and (f) (Tl, Au)/Si(100) $c(2 \times 2)$ compound. In the LEED patterns, the main spots are outlined by the open red circles, and the reciprocal lattice unit cells are outlined by the dashed blue lines to guide the eye. The tunneling parameters: -2.0 V, 1.2 nA for (b) and (d) and -0.8 V, 1.0 nA for (f).

The final structural model of the (Tl, Au)/Si(100) $c(2 \times 2)$ compound is shown in Fig. 2(a). It has essentially a distinct double-atomic-layer structure where Au atoms [shown by the yellow balls in Fig. 2(a)] constitute the bottom layer, whereas the top layer is built of Tl atoms [the gray balls in Fig. 2(a)]. The Au layer resides 1.42 Å higher than the top Si(100) layer, and the Tl layer is 1.57 Å above the Au layer. One can note that Au atoms within the atomic row running along the $[\bar{1}10]$ direction parallel to the original direction of Si-dimer rows are not spaced equidistantly. The fragment of the bare Si(100) 2×1 surface is shown in the upper left corner of the ball-and-stick model in Fig. 2(a). The Au-Au distances vary alternatively between 3.30 and 4.43 Å. One could think about a kind of atomic dimerization, but the bulk Au-Au bond length is much less, 2.88 Å. The neighboring Au atomic rows are arranged in a way to form a $c(2 \times 2)$ (i.e., $\sqrt{2} \times \sqrt{2}$ - $R45^\circ$) 2D lattice. The Tl atoms are dimerized in the orthogonal $[110]$ direction with spacings of 3.44 and

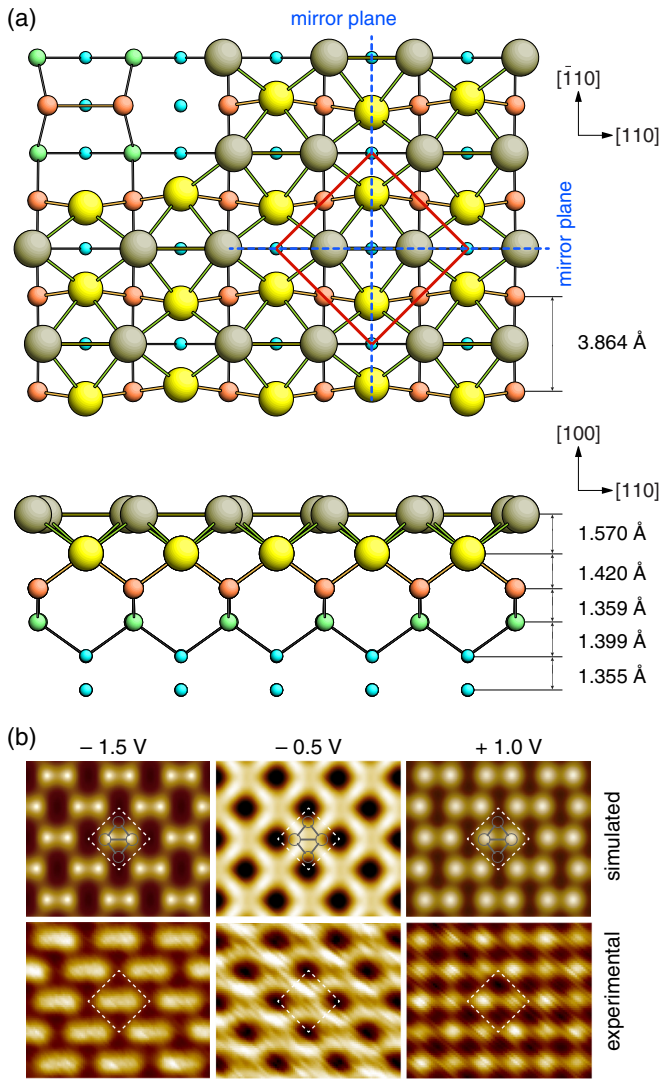


FIG. 2. (a) Ball-and-stick model of the (Tl, Au)/Si(100)c(2 × 2) structure (top and side views). Au atoms are shown by yellow balls, Tl atoms are shown by gray balls, and Si atoms are shown by orange, green, and blue balls, depending on the layer. The primitive $\sqrt{2} \times \sqrt{2}$ -R45° cell is outlined by the red square. The horizontal and vertical dashed lines indicate the mirror planes. (b) Comparison of the simulated (upper panel) and experimental (lower panel) STM images acquired at -1.5-, -0.5-, and +1.0-V sample bias voltages.

4.29 Å. Thus, the resultant (Tl, Au)/Si(100) structure has a c(2 × 2) 2D lattice with the basis having a C_{2v} symmetry (plane-group $p2mm$). Note that the presence of the Tl-Au layer does not reduce the Si(100) substrate symmetry. To check the validity of the model, its simulated STM images were compared with their experimental counterparts. One can see a clear correspondence between them at various bias voltages [Fig. 2(b)] that can serve as an argument in favor of the proposed model. The minor difference between simulated and experimental STM images at +1.0-V bias (protrusions are dimerized in the former but not in the latter) can be ascribed to the dynamic behavior of surface Tl atoms.

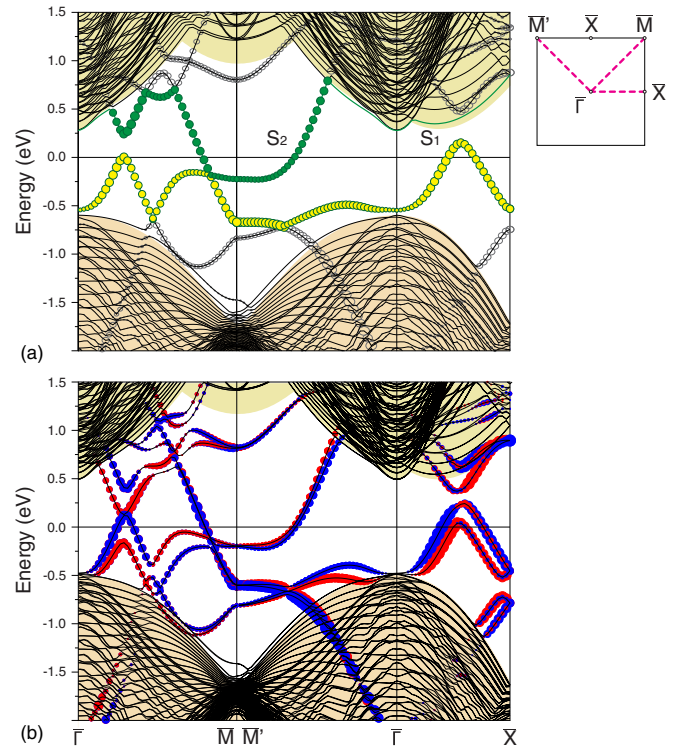


FIG. 3. Electronic band structure of the (Tl, Au)/Si(111)c(2 × 2) surface calculated (a) without and (b) with considering SOC contribution. The bands crossing E_F , S_1 and S_2 , in (a) are highlighted by yellow and green circles, respectively. The bands with opposite spin orientation in (b) are highlighted by blue and red circles. The size of the circle corresponds to the strength of the surface character summed over all orbitals at a particular k_{\parallel} value. The shaded region indicates projected bulk bands. The $\sqrt{2} \times \sqrt{2}$ SBZ with the indicated high-symmetry points is shown in the top right corner. The dashed red lines indicate the passes along which the dispersions were calculated. The LDA and 60 Si SL slabs were used.

Having a proper structural model of (Tl, Au)/Si(100)c(2 × 2), we can explore its electronic properties in detail. Figure 3 presents an electronic band structure calculated along the high-symmetry directions of the $\sqrt{2} \times \sqrt{2}$ SBZ when SOC is ignored [Fig. 3(a)] and when it is taken into account [Fig. 3(b)]. Due to the C_{2v} symmetry of the (Tl, Au)/Si(100)c(2 × 2) surface, its bands coincide along all $\bar{\Gamma}$ - \bar{X} directions, whereas they are not equivalent along the $\bar{\Gamma}$ - \bar{M} and $\bar{\Gamma}$ - \bar{M}' directions. In the spectrum with switched-off SOC [Fig. 3(a)], one can see the two surface-state bands, noted S_1 and S_2 , in the Si(100) band-gap region. They cross the Fermi level and are responsible for the metallic properties of the 2D Tl-Au compound. Due to the lack of inversion symmetry in the metallic film, these bands demonstrate a Rashba-type spin splitting in the relativistic spectrum [Fig. 3(b)]. Splittings at the Fermi level are the largest for the S_1 hole pocket, and their values are 0.06 and 0.09 Å⁻¹ in momentum and 200 and 270 meV in energy. For the S_2 electron pocket, they are much smaller, 0.002 Å⁻¹ and 7 meV in the $\bar{\Gamma}$ - \bar{M} direction and 0.02 Å⁻¹ and 60 meV in

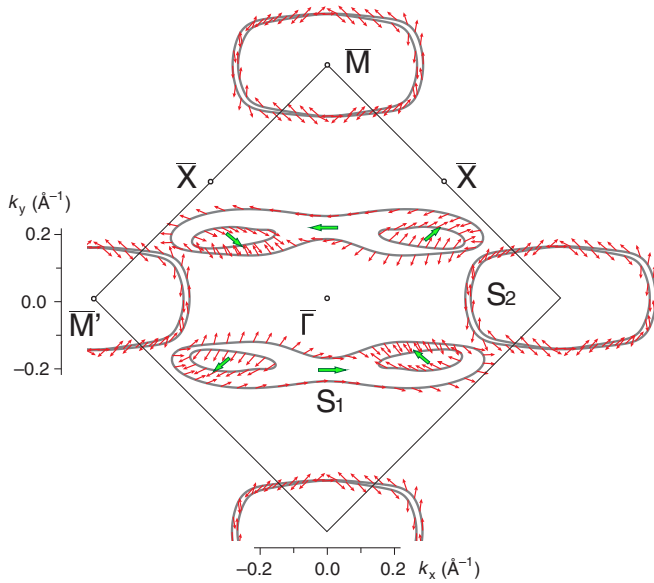


FIG. 4. Calculated Fermi-contour map of the (Tl, Au)/Si(111)c(2 × 2) surface where the red arrows adjacent to the contours and their lengths denote the in-plane spin component. The green arrows show the net spin for each Fermi contour for the S_1 bands. The $\sqrt{2} \times \sqrt{2}$ SBZ is outlined.

the $\bar{\Gamma}$ - \bar{M}' direction. The orbital composition of these surface bands is determined by the mixture of the s and p states of Tl and the p and d states of Au with negligible contribution of the s states of Au. All Tl p_x , p_y , and p_z states contribute to the composition of both S_1 and S_2 bands, whereas the Tl s -state contribution is comparable with that of the Tl p states only for the S_2 band. With regard to the Au p states, mainly the p_x and p_y states contribute to the S_1 band, whereas the p_z states contribute mainly to the S_2 band. Au d states contribute to both bands whereas d_{xz} and d_{yz} orbitals are present in the S_1 band, and d_{xy} and d_{z^2} orbitals contribute to the S_2 band.

Figure 3(b) shows the in-plane spin components, whereas all the out-of-plane spin components are identically zero. The absence of the out-of-plane spin components is the distinctive feature of the (Tl, Au)/Si(100)c(2 × 2) 2D compound, and it is determined by the symmetry of the system which, in turn, is determined by the substrate symmetry. The absence of the out-of-plane spin component can be easily understood if one considers an ideal 2D system with a C_{2v} group symmetry. Indeed, the time-reversal symmetry operation changes the sign of the normal projection of the electron spin $s_z(k_x, k_y) \rightarrow -s_z(-k_x, -k_y)$, whereas 180° in-plane rotation does not change it, i.e., $s_z(k_x, k_y) \rightarrow s_z(-k_x, -k_y)$. Then, $s_z(-k_x, -k_y) = -s_z(-k_x, -k_y) \equiv 0$ for any k_x and k_y .

Figure 4 shows the constant-energy contours calculated for the energy cut corresponding to the Fermi level. The S_2 band forms two concentric contours having the shape of a rounded rectangle around the \bar{M} (\bar{M}') points. Their in-plane spin components follow, in general, the behavior typical for Rashba helicity, namely, the clockwise/counterclockwise rotation in the outer/inner contours. On the other hand, the

spin-split S_1 band gives rise to the emergence of a pair of beanpodlike features in the Fermi-contour map. These two contour features, consisting of outer warped-elliptical-shaped and two inner bean-shaped contours, are not centered at any time-reversal invariant momenta and are symmetric with respect to the $[\bar{1}10]$ mirror plane. The net spin of the outer contours is pointed along the k_x direction. The s_x component is positive for the outer contour on the $k_y < 0$ half-plane, and it is negative in its counterpart on the $k_y > 0$ half-plane. The s_x components of the net spin in the inner contours are antiparallel to that in the outer contours. Along with this, the s_y components are antiparallel in each pair of inner contours. Thus, the spin texture of the S_1 band is nonvortical. The origin of the nonvortical spin texture of the S_1 states is related with the fact that the constant energy contours are not centered at any time-reversal invariant momenta point (see Fig. 4). As was demonstrated by Oguchi and Shishidou [19] 2D states belonging to C_{2v} symmetry may not be isotropic or vortical, depending on the anisotropic character of the relevant surface states. The symmetry of our system is C_{2v} , and hence it can comprise 2D states with nonvortical spin textures. Indeed we found that of the two surface-state bands in (Tl, Au)/Si(100)c(2 × 2), one, S_2 , has a typical vortical spin texture, whereas the other, S_1 , demonstrates an unusual nonvortical spin texture.

In order to compare the calculated band structure with an experimental spectrum, it is necessary to take into account that the grown (Tl, Au)/Si(111)c(2 × 2) compound has a two-domain structure since neighboring terraces of the Si(100) surface are rotated by 90° to each other. Consequently, the ARPES spectrum should reflect the superposition from the two rotational domains. The ARPES measurements were performed along the $\bar{\Gamma}$ - \bar{X} direction where the contribution from the two domains is identical and along the $\bar{\Gamma}$ - \bar{M} directions where it is not (see inset in Fig. 3). In the later case, the two inequivalent contributions along the $\bar{\Gamma}$ - \bar{M} and $\bar{\Gamma}$ - \bar{M}' directions are superimposed [see Fig. 5(a) for the ARPES spectrum]. In the calculated band structure in order to compare it with the experimental ARPES spectrum, we also overlaid the $\bar{\Gamma}$ - \bar{M} and $\bar{\Gamma}$ - \bar{M}' directions [Fig. 5(b)]. As can be realized from the comparison of experimental and LDA surface spectra, the coincidence between them near the Fermi level is fairly good. However, the dispersion of the deep-lying surface bands at -0.4 to -0.8 eV in the $\bar{\Gamma}$ - \bar{M}' direction in the calculated band structure is a little bit different than in the experimental spectrum. We also calculated the surface band structure by using the HSE06 hybrid exchange-correlation functional which is believed to be more accurate in the band-structure description [Fig. 5(c)]. As can be seen the spectrum calculated within the HSE06 approach perfectly reproduces the experimental data, and at the Fermi level its difference from the LDA spectrum consists only of a slightly smaller spin splitting of the S_1 band in the $\bar{\Gamma}$ - \bar{X} direction.

Figure 6 allows for comparing the experimental (upper panel) and calculated (lower panel) Fermi contours of the (Tl, Au)/Si(100)c(2 × 2) surface. The calculated contours for the two domains are shown with white and orange colors, and the boundaries of the $\sqrt{2} \times \sqrt{2}$ SBZs are shown with thin gray line. The resultant energy map is essentially a

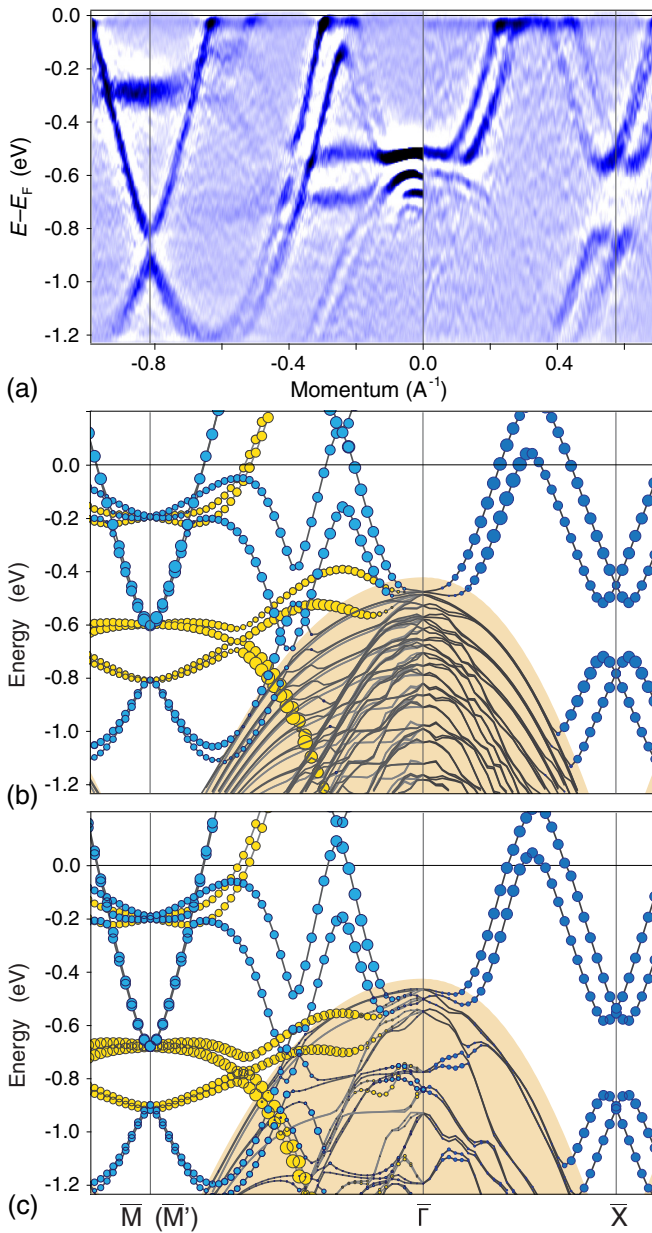


FIG. 5. Comparison of the measured ARPES spectrum of the (a) (Tl, Au)/Si(111)c(2 × 2) surface with theoretical results obtained within the (b) LDA, and the (c) HSE06 calculations. In the calculated band structures, the inequivalent $\bar{\Gamma}-\bar{M}$ and $\bar{\Gamma}-\bar{M}'$ directions are superimposed, and the corresponding dispersions are shown by circles of different colors, yellow and blue.

superposition of the contributions from the two rotational domains repeated periodically with a translation of the $\sqrt{2} \times \sqrt{2}$ SBZ. Although the obtained experimental pattern looks quite complicated, one can note a remarkable coincidence between experimental and calculated maps. Every fine feature in the experimental map has its counterpart in the calculated map and vice versa. This clear correspondence as well as the correspondence of the calculated band structure and experimentally obtained ARPES spectrum can serve as a solid argument for a validity of the proposed (Tl, Au)/Si(100)c(2 × 2) structural model.

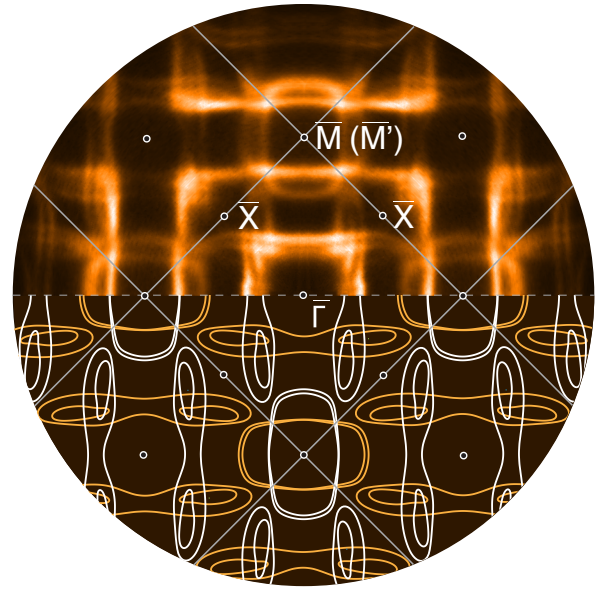


FIG. 6. Experimental (upper panel) and calculated (lower panel) Fermi-contour maps of the (Tl, Au)/Si(111)c(2 × 2) surface. The thin gray lines indicate the boundaries of the $\sqrt{2} \times \sqrt{2}$ SBZs. In the calculated map, the contributions from the two rotational domains are shown by the white and orange colors.

IV. CONCLUSIONS

In conclusion, using a combination of the experimental techniques, including LEED, STM, and ARPES together with the DFT calculations we have characterized the structural and electronic properties of the (Tl, Au)/Si(100)c(2 × 2) 2D compound which is formed upon adsorption of 1.0 ML of Au onto the Tl/Si(100)2 × 1 surface with 1.0 ML of Tl held at RT. The (Tl, Au)/Si(100)c(2 × 2) compound has been determined to have a double-atomic-layer structure where Au and Tl atoms constitute the bottom and top layers, respectively. The compound is metallic due to the presence of two dispersive surface-state bands crossing the Fermi level. Both bands are spin split, and their all out-of-plane spin components are zero, that stems from the C_{2v} symmetry of the system. However, only the spin-resolved ARPES data could demonstrate unambiguously that this is held for any k point of the SBZ. Of the two surface-state bands, one has a typical vortical spin texture, whereas the other demonstrates an unusual nonvortical spin texture. Bearing in mind that the nonvortical spin texture is supposed to suppress the backscattering of the spin carriers [5,18], the (Tl, Au)/Si(100)c(2 × 2) compound might be thought to be potentially more promising as compared to the well-studied C_{3v} 2D Rashba systems.

ACKNOWLEDGMENTS

The work was supported by the Russian Science Foundation under Grant No. 14-12-00479-P. The calculations were conducted using the equipment of the Shared Resource Center “Far Eastern Computing Resource” IACP FEB RAS [33].

- [1] E. I. Rashba, *Sov. Phys. Solid State* **2**, 1109 (1960).
- [2] Y. A. Bychkov and E. I. Rashba, *JETP Lett.* **39**, 78 (1984).
- [3] K. Sakamoto, T. Oda, A. Kimura, K. Miyamoto, M. Tsujikawa, A. Imai, N. Ueno, H. Namatame, M. Taniguchi, P. E. J. Eriksson, and R. I. G. Uhrberg, *Phys. Rev. Lett.* **102**, 096805 (2009).
- [4] J. Ibañez-Azpiroz, A. Eiguren, and A. Bergara, *Phys. Rev. B* **84**, 125435 (2011).
- [5] K. Sakamoto, T.-H. Kim, T. Kuzumaki, B. Müller, Y. Yamamoto, M. Ohtaka, J. R. Osiecki, K. Miyamoto, Y. Takeichi, A. Harasawa, S. D. Stolwijk, A. B. Schmidt, J. Fujii, R. I. G. Uhrberg, M. Donath, H. W. Yeom, and T. Oda, *Nat. Commun.* **4**, 1 (2013).
- [6] S. D. Stolwijk, A. B. Schmidt, M. Donath, K. Sakamoto, and P. Krüger, *Phys. Rev. Lett.* **111**, 176402 (2013).
- [7] S. D. Stolwijk, K. Sakamoto, A. B. Schmidt, P. Krüger, and M. Donath, *Phys. Rev. B* **90**, 161109 (2014).
- [8] K. Sakamoto, T. Oda, A. Kimura, Y. Takeichi, J. Fujii, R. I. G. Uhrberg, M. Donath, and H. W. Yeom, *J. Electron Spectrosc. Relat. Phenom.* **201**, 88 (2015).
- [9] K. Nakajin and S. Murakami, *Phys. Rev. B* **91**, 245428 (2015).
- [10] S. D. Stolwijk, K. Sakamoto, A. B. Schmidt, P. Krüger, and M. Donath, *Phys. Rev. B* **91**, 245420 (2015).
- [11] S. D. Stolwijk, A. B. Schmidt, K. Sakamoto, P. Krüger, and M. Donath, *Phys. Rev. Mater.* **1**, 064604 (2017).
- [12] P. Garcia-Goiricelaya, I. G. Gurtubay, and A. Eiguren, *Phys. Rev. B* **97**, 201405 (2018).
- [13] I. Gierz, T. Suzuki, E. Frantzeskakis, S. Pons, S. Ostanin, A. Ernst, J. Henk, M. Grioni, K. Kern, and C. R. Ast, *Phys. Rev. Lett.* **103**, 046803 (2009).
- [14] K. Sakamoto, H. Kakuta, K. Sugawara, K. Miyamoto, A. Kimura, T. Kuzumaki, N. Ueno, E. Annese, J. Fujii, A. Kodama, T. Shishidou, H. Namatame, M. Taniguchi, T. Sato, T. Takahashi, and T. Oguchi, *Phys. Rev. Lett.* **103**, 156801 (2009).
- [15] E. Frantzeskakis, S. Pons, and M. Grioni, *Phys. Rev. B* **82**, 085440 (2010).
- [16] M. H. Berntsen, O. Götberg, and O. Tjernberg, *Phys. Rev. B* **97**, 125148 (2018).
- [17] J. Park, S. W. Jung, M. C. Jung, H. Yamane, N. Kosugi, and H. W. Yeom, *Phys. Rev. Lett.* **110**, 036801 (2013).
- [18] E. Annese, T. Kuzumaki, B. Müller, Y. Yamamoto, H. Nakano, H. Kato, A. Araki, M. Ohtaka, T. Aoki, H. Ishikawa, T. Hayashida, J. R. Osiecki, K. Miyamoto, Y. Takeichi, A. Harasawa, K. Yaji, T. Shirasawa, K. I. Nittoh, W. Yang, K. Miki, T. Oda, H. W. Yeom, and K. Sakamoto, *Phys. Rev. Lett.* **117**, 016803 (2016).
- [19] T. Oguchi and T. Shishidou, *J. Phys.: Condens. Matter* **21**, 092001 (2009).
- [20] K. Yaji, Y. Ohtsubo, S. Hatta, H. Okuyama, K. Miyamoto, T. Okuda, A. Kimura, H. Namatame, M. Taniguchi, and T. Aruga, *Nat. Commun.* **1**, 17 (2010).
- [21] D. V. Gruznev, L. V. Bondarenko, A. V. Matetskiy, A. A. Yakovlev, A. Y. Tupchaya, S. V. Eremeev, E. V. Chulkov, J.-P. Chou, C.-M. Wei, M.-Y. Lai, Y.-L. Wang, A. V. Zotov, and A. A. Saranin, *Sci. Rep.* **4**, 04742 (2014).
- [22] D. V. Gruznev, A. V. Zotov, and A. A. Saranin, *Jpn. J. Appl. Phys.* **56**, 08LA01 (2017).
- [23] G. Kresse and J. Hafner, *Phys. Rev. B* **47**, 558 (1993).
- [24] G. Kresse and D. Joubert, *Phys. Rev. B* **59**, 1758 (1999).
- [25] P. E. Blöchl, *Phys. Rev. B* **50**, 17953 (1994).
- [26] J. P. Perdew and A. Zunger, *Phys. Rev. B* **23**, 5048 (1981).
- [27] C. J. Pickard and R. J. Needs, *J. Phys.: Condens. Matter* **23**, 053201 (2011).
- [28] J. Heyd, G. E. Scuseria, and M. Ernzerhof, *J. Chem. Phys.* **118**, 8207 (2003).
- [29] L. G. Ferreira, M. Marques, and L. K. Teles, *Phys. Rev. B* **78**, 125116 (2008).
- [30] L. G. Ferreira, M. Marques, and L. K. Teles, *AIP Adv.* **1**, 032119 (2011).
- [31] A. A. Saranin, A. V. Zotov, V. G. Kotlyar, I. A. Kuyanov, T. V. Kasyanova, A. Nishida, M. Kishida, Y. Murata, H. Okado, M. Katayama, and K. Oura, *Phys. Rev. B* **71**, 035312 (2005).
- [32] P. E. J. Eriksson, K. Sakamoto, and R. I. G. Uhrberg, *Phys. Rev. B* **81**, 205422 (2010).
- [33] <https://cc.dvo.ru>